Letter

High-energy spin excitations in the quantum spin liquid candidate Zn-substituted barlowite probed by resonant inelastic x-ray scattering

Rebecca W. Smaha,[1,2,*] Jonathan Pelliciari,[3] Ignace Jarrige,[3] Valentina Bisogni,[3] Aaron T. Breidenbach,[1,4] Jack Mingde Jiang,[1,5] Jiajia Wen,[1] Hong-Chen Jiang,[1] and Young S. Lee[1,5,†]

[1]*Stanford Institute for Materials and Energy Sciences, SLAC National Accelerator Laboratory, Menlo Park, California 94025, USA*

[2]*Department of Chemistry, Stanford University, Stanford, California 94305, USA*

[3]*National Synchrotron Light Source II, Brookhaven National Laboratory, Upton, New York 11973, USA*

[4]*Department of Physics, Stanford University, Stanford, California 94305, USA*

[5]*Department of Applied Physics, Stanford University, Stanford, California 94305, USA*

(Received 25 August 2021; revised 1 December 2022; accepted 4 January 2023; published 3 February 2023)

A quantum spin liquid is a novel ground state that can support long-range entanglement between magnetic moments, resulting in exotic spin excitations involving fractionalized $S = \frac{1}{2}$ spinons. Here, we measure the excitations in single crystals of the spin liquid candidate Zn-barlowite using resonant inelastic x-ray scattering. By analyzing the incident polarization and temperature dependences, we deduce a clear magnetic scattering contribution forming a broad continuum that surprisingly extends up to ∼200 meV (∼14J, where J is the magnetic exchange). The excitation spectrum indicates that significant contributions may arise from multiple pairs of spinons and/or antispinons at high energies. Furthermore, the observation of similar scattering in the hexagonal barlowite parent material above its ordering temperature suggests the presence of similar high-energy excitations, irrespective of the low-energy physics.

DOI: 10.1103/PhysRevB.107.L060402

A fascinating phenomenon in quantum magnets is the possibility of having magnetic excitations with fractional quantum numbers. In particular, this may occur in a quantum spin liquid (QSL), which is characterized by long-range quantum entanglement of the spins in the absence of long-range magnetic order [1–3]. Here, the fundamental $\Delta S = 1$ excitations may fractionalize into pairs of $S = \frac{1}{2}$ spinons. A promising host of a QSL is the kagome lattice of corner-sharing triangles with magnetically frustrated antiferromagnetic spin-$\frac{1}{2}$ moments [4–13]. A preeminent kagome QSL candidate is the mineral herbertsmithite [$Cu_3Zn(OH)_6Cl_2$]; however, a small percentage of excess Cu^{2+} impurities are found on the nonmagnetic Zn^{2+} sites between the kagome layers [14–18]. While these defects may affect the low-energy physics ($<J/10$, where $J \approx 14$ meV is the magnetic exchange energy), the high-energy spin excitations should be relatively unaffected. Furthermore, comparing the QSL with its closely related parent compound with long-range magnetic order can provide insight into the universal high-energy quantum spin dynamics of QSL candidates and proximal phases.

The spin-$\frac{1}{2}$ kagome material Zn-substituted barlowite [$Cu_3Zn_xCu_{1-x}(OH)_6FBr$] was recently identified as a QSL candidate that has a different impurity environment and layer stacking arrangement compared to herbertsmithite [19–22]. We synthesized single crystals of Zn-barlowite; they have a Zn substitution of $x = 0.56$, referred to as $Zn_{0.56}$ [21]. Its hexagonal structure is shown in Fig. S1 in the Supplemental Material (SM)[23]: The kagome layers are fully occupied by Cu^{2+}, while the interlayers have a majority of nonmagnetic Zn^{2+} ions interspersed with Cu^{2+} impurities [22]. $Zn_{0.56}$ has no long-range magnetic order down to $T = 0.1$ K, making it a good QSL candidate [21]. However, the lack of large single crystals has impeded measurements of the spinon physics with neutron scattering, a technique which provides high-energy resolution and a well-defined cross section for scattering from $\Delta S = 1$ excitations.

Resonant inelastic x-ray scattering (RIXS) offers a unique opportunity to study this kagome QSL candidate. RIXS is a powerful probe of elementary electronic excitations, including magnetic excitations, and has the capability of measuring small single crystals (<1 mm in length) [24–27]. Furthermore, RIXS naturally probes significantly higher-energy transfers than neutrons and has a different sensitivity to excitations. For magnetic scattering, the RIXS cross section may detect $\Delta S = 0$ as well as $\Delta S = 1$ excitations, and therefore can probe excitations that evade neutrons [25,28]. While the application of RIXS to materials with low-energy or overlapping excitations has been limited by the energy resolution, significant advances have recently improved the achievable resolution to 15–30 meV for soft x rays. Recent experimental and computational advances in RIXS have focused on compounds with one-dimensional (1D) chains or two-dimensional (2D) square lattices of Cu^{2+} [25,29–32], as well as honeycomb lattice materials [33–36]. However, even though kagome quantum magnets with Cu^{2+} cations display many interesting physical phenomena, experimental RIXS investigations are lacking.

*Present address: Materials Science Center, National Renewable Energy Laboratory, Golden, Colorado 80401, USA; rsmaha@alumni.stanford.edu

†youngsl@stanford.edu

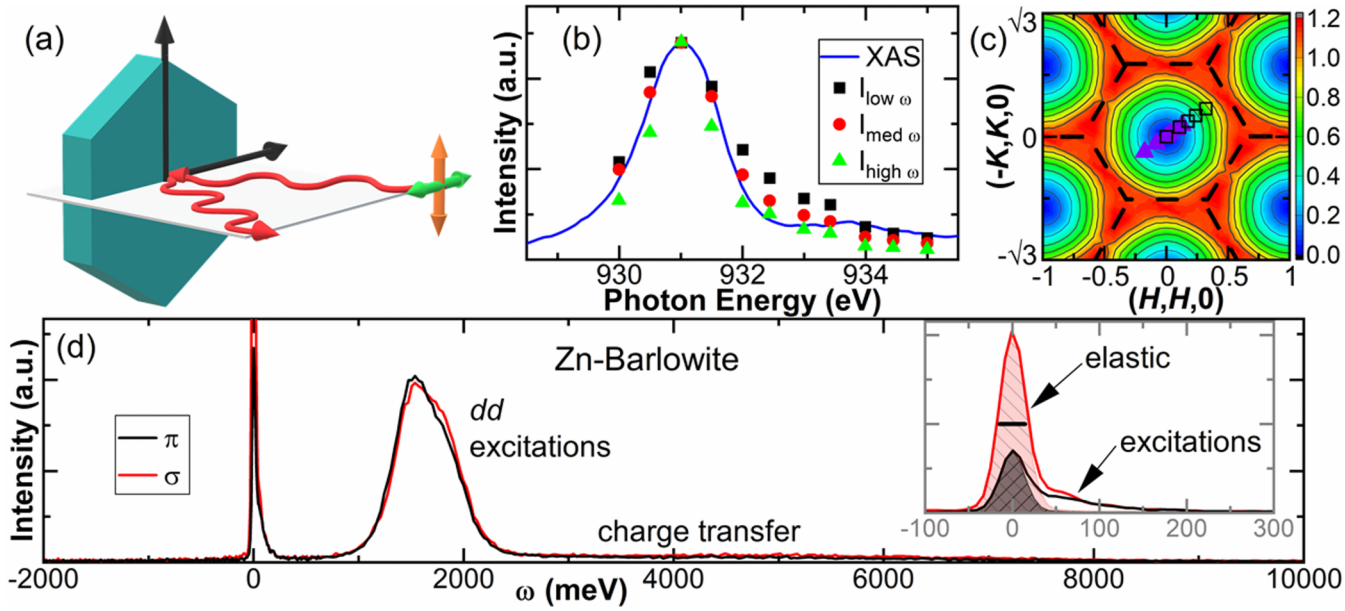

FIG. 1. (a) Schematic of the sample orientation on the beamline showing the $(H0L)$ scattering plane and the π- or σ-polarization directions. (b) Integrations of the incident photon energy dependence heat maps at a variety of energy loss (ω) ranges ($I_{\mathrm{low}\,\omega} = -40$–$40$ meV; $I_{\mathrm{med}\,\omega} = 40$–$120$ meV; $I_{\mathrm{high}\,\omega} = 120$–$200$ meV), plotted with the XAS collected for barlowite 2. The integrations and XAS have been normalized. For details and Zn-barlowite $Zn_{0.56}$ data, see Figs. S5 and S6 in the SM. (c) Calculated static spin structure factor $S(\mathbf{q}, S_z)$ with total spin $S_z = 0$. The Brillouin zone is depicted with dashed lines, and the measured $q_\parallel$ locations are shown as purple triangles and black squares for scattering angles $2\theta = 90^\circ$ and 150°, respectively. (d) RIXS signal of Zn-barlowite $Zn_{0.56}$ at $(q_\parallel, q_\perp) = (0, 1.0)$ collected in both π and σ polarizations. The band of dd excitations is visible between $\sim$1 and 2.5 eV, and charge transfer scattering is visible as a broad hump between $\sim$3 and 6 eV. The inset magnifies the region near $\omega = 0$ meV showing the elastic component and inelastic scattering. The black bar represents the instrumental resolution (29 meV). The elastic components were fit with pseudo-Voigt line shapes denoted by the shaded area (see SM Sec. I E). The data were collected at $T = 30$ K and $2\theta = 90^\circ$

We present RIXS measurements on small single crystals of the kagome QSL candidate Zn-barlowite $Zn_{0.56}$ [21]. RIXS data were collected on beamline 2-ID at the NSLS II at Brookhaven National Laboratory at the Cu L_3 edge ($\sim$930 eV) [35,37]. The scattering geometry is shown schematically in Fig. 1(a). X-ray absorption spectroscopy confirms the presence of Cu^{2+} [Figs. 1(b) and S2]. Integrating the incident photon energy-dependent data across several energy loss (ω) ranges shows that the observed signal is resonantly enhanced [Figs. 1(b), S4, and S5]. We collected RIXS data at a scattering angle of $2\theta = 90^\circ$ in both π and σ incoming photon polarizations. All data were normalized by the area of the dd excitations. At $2\theta = 90^\circ$ with π polarization, the elastic charge scattering and phonon scattering should be suppressed relative to the magnetic scattering. However, precise quantification may be complicated by the lower point group symmetry of the kagome Cu^{2+} d orbitals compared to square lattice cuprates [38]. Figure 1(d) shows a wide energy loss (ω) range of the data, where scattering from the dd excitations is visible between 1 and 2.5 eV, and charge transfer scattering is present as a broad, weak peak centered at $\sim$4 eV. The energy resolution, shown as the black bar in the inset of Fig. 1(d), was approximately 29 meV. The inset magnifies the region near $\omega = 0$ meV, showing the suppression of the elastic line in π polarization compared to σ polarization. After fitting the elastic component with a pseudo-Voigt (shaded in the inset), we observed inelastic scattering extending up to approximately 200 meV.

For this quasi-2D material, $\vec{q}$ can be decomposed into in-plane and out-of-plane components $(q_\parallel, q_\perp)$. Here, $q_\parallel$ is along $(H, 0, 0)$, and $q_\perp$ is along $(0, 0, L)$ (see Fig. S3). For weakly coupled layers, the scattering at high energies depends primarily on $q_\parallel$ within the kagome layer and is weakly dependent on (or independent of) $q_\perp$. Subtracting the elastic component reveals the inelastic scattering as a broad continuum in Figs. 2(a) and 2(b). The lack of any sharp components suggests that scattering from individual phonon modes is weak under these experimental conditions [24], although there may be some contribution within the energy range of the continuum (Fig. S9). We fit the inelastic scattering with a damped harmonic oscillator (DHO) cross section (see SM Sec. I E), which provides a qualitatively good description of the data. The fitted width (Γ) and integrated intensity are weakly dependent on $q_\parallel$ and are plotted in Figs. 2(e) and 2(f), respectively. The π-polarized data, which should be less affected by the charge scattering, has a consistently higher integrated intensity than the σ-polarized data, indicating that the continuum likely has a substantial magnetic component.

To measure larger wave vectors, we also collected data at $2\theta = 150^\circ$ [Figs. 2(c) and 2(d)]. The elastic component was fit and subtracted as before (SM Sec. I F), and we noted an interesting decrease of this (quasi)elastic component upon warming to 300 K [Figs. S6(c) and S10] which may originate from diffuse structural scattering [39]. The inelastic scattering at $T = 30$ K has a broad tail that extends up to $\sim$200 meV, consistent with that at $2\theta = 90^\circ$. At $T = 300$ K,

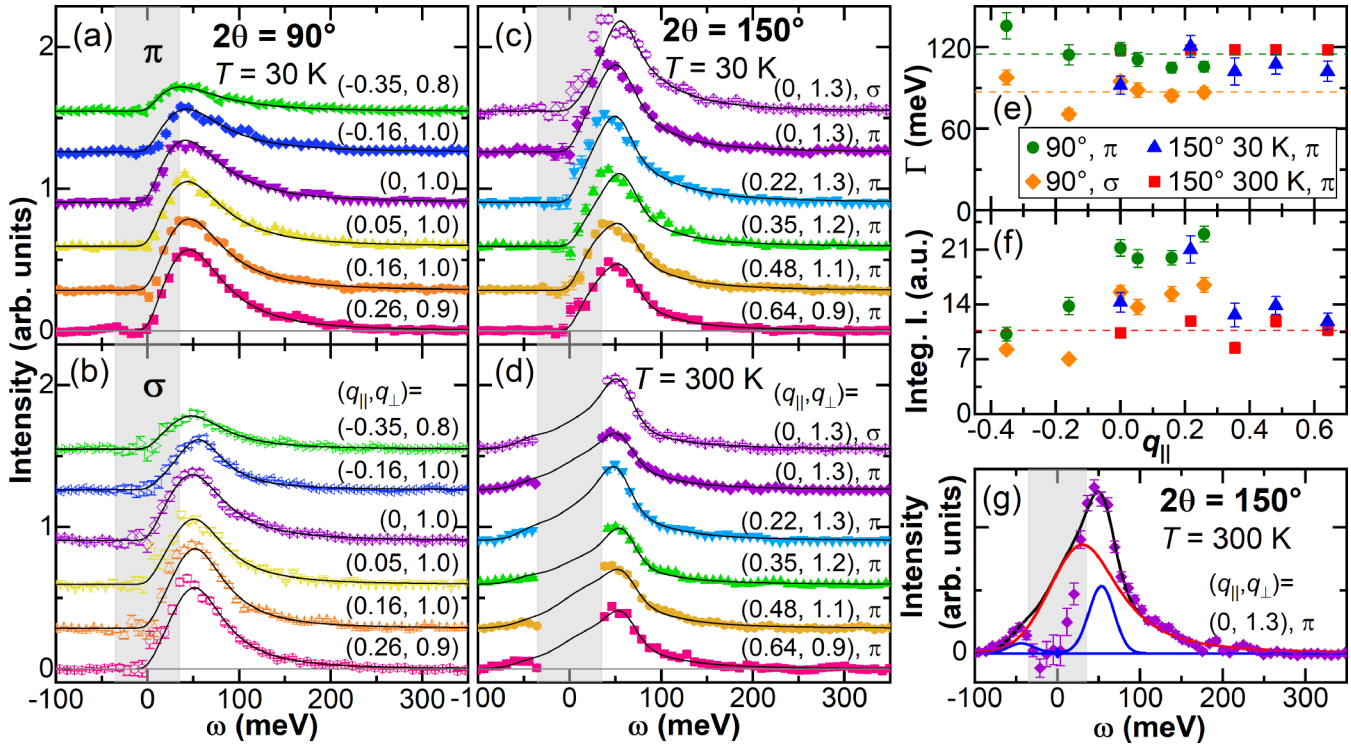

FIG. 2. (a), (b) The q dependence of the inelastic scattering of Zn-barlowite $Zn_{0.56}$ collected at $T = 30$ K and scattering angle $2\theta = 90°$ in both (a) π and (b) σ polarizations. (c), (d) The q dependence of the inelastic scattering of $Zn_{0.56}$ collected at (c) $T = 30$ K and (d) $T = 300$ K at $2\theta = 150°$. Both σ (open symbols) and π (solid symbols) polarizations are shown. In (a) and (b), the data were fit with a damped harmonic oscillator (DHO) curve from -100 to 500 meV with the DHO center fixed at 65 meV. In (c) and (d), the data were fit with a DHO and a phonon mode (see SM Sec. I F) from -100 to 500 meV; full $T = 300$ K data are in Fig. S17. The best fits are shown as black lines. The shading denotes in (a) and (b) a region of high uncertainty due to the elastic subtraction and in (c) and (d) regions that were masked during fitting. Vertical offsets were applied to separate the spectra. (e), (f) The fitted DHO width Γ and integrated intensity as a function of $q_\parallel$. In (e), Γ for the $T = 300$ K fits was fixed at 119 meV, as described in SM Sec. I F. Horizontal dashed lines denote average values. (g) An example of the "DHO+phonon" model showing the fit components (red and blue lines, respectively) and the overall fit (black line).

the high-energy scattering is somewhat reduced, revealing a more well-defined peak near 60 meV that is likely due to phonons, as this energy is consistent with previously calculated phonon modes [40]. We therefore fit the $2\theta = 150°$ data at both temperatures with a model consisting of a DHO and a phonon mode (see SM Secs. I F and II). As seen in the individual fit components drawn in Fig. 2(g), when the phonon mode is taken into account a DHO with similar parameters as previously determined at $T = 30$ K at both $2\theta = 90°$ and $150°$ describes the remaining continuum. The integrated intensities of the $T = 30$ K data in Fig. 2(f) have a weak maximum at small $q_\parallel$ values. In contrast, the room-temperature intensities are relatively suppressed and are flat across $q_\parallel$. Thus, if the broad continuum is magnetic in origin, then the spin correlations grow upon cooling, as would generally be expected.

To further investigate the magnetic origin of the signal, we divided the total inelastic scattering by the thermal factor $[n(\omega) + 1]$. Hence, if the inelastic scattering is proportional to $S(q, w)F(q, w)$, where $F(q, w)$ is a temperature-independent form factor, then the phonon "background" contribution to the resultant imaginary part of the general susceptibility, χ'', should not change much between these temperatures (see SM Sec. V). Therefore the change in $\chi''F$ between high and low temperature should be mostly magnetic in origin, and this comparison is plotted in Fig. 3(a). Again, the signal is clearly stronger at low temperatures, indicating enhanced spin correlations. (If spin-phonon interactions are relevant, the phonon dynamics may also evolve with the spin correlations.) A larger temperature difference is seen at small $q_\parallel$; we therefore plot the quantity $\chi''F_{T=30\,\mathrm{K}} - \chi''F_{T=300\,\mathrm{K}}$ in Fig. 3(b) for $q_\parallel = 0$. Figure 3(c) shows the $q_\parallel$-dependent subtraction $\chi''F_{q_\parallel=0} - \chi''F_{q_\parallel=0.64}$ at $T = 30$ K, revealing a weak $q_\parallel$ dependence to the low-temperature scattering.

Thus, both the polarization and temperature dependences of the inelastic scattering suggest the presence of a magnetic continuum up to ~200 meV (~$14J$). The spectrum may be empirically described by an overdamped harmonic oscillator (with $\Gamma \approx 110$ meV $> \omega_0 \approx 65$ meV). Due to the instrumental resolution of 29 meV, we cannot accurately determine any possible power-law or exponential dependence of the intensity near $\omega = 0$ meV. The RIXS data cannot resolve the question of gapless versus gapped spin excitations, but rather provide results in the high-energy regime, above the range probed by neutron scattering techniques.

Because $Zn_{0.56}$ does not have long-range magnetic order at any measured temperature, the broad continuum does not originate from scattering from conventional magnons. Perhaps one could consider multimagnon scattering from regions with short-range spin correlations. However, the evidence for QSL behavior [21] in these samples leads to an

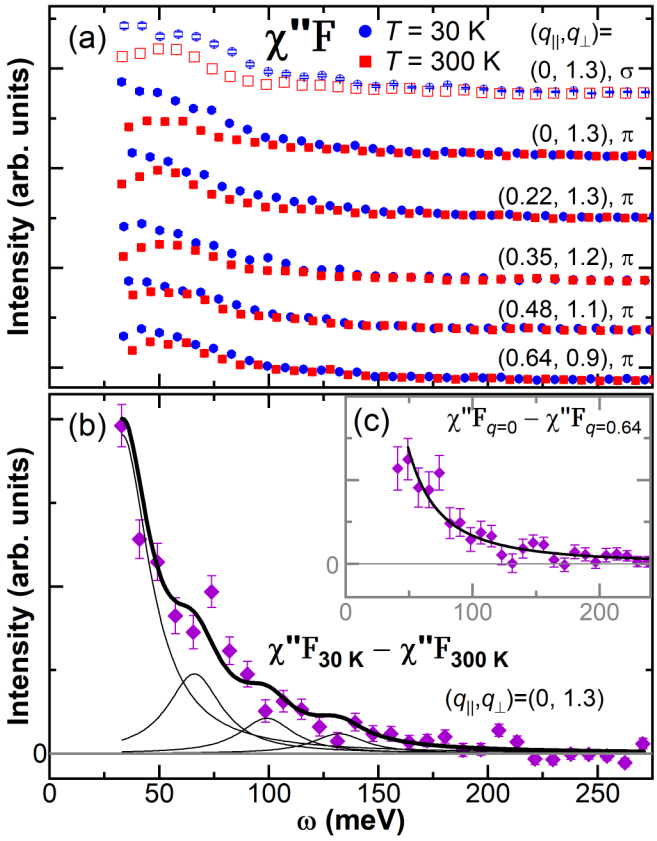

FIG. 3. (a) The q dependence of the susceptibility times the form factor ($\chi''F$) of Zn-barlowite $Zn_{0.56}$ at $T = 30$ K and $T = 300$ K. Vertical offsets were applied to separate the spectra. (b) Enhancement of $\chi''F$ at low temperature and π polarization for $q_\parallel = 0$. A series of Lorentzians representing single and multiple pairs of spinon excitations (thin lines) and their sum (thick line) are overlaid. Additional q values are shown in Fig. S15. (c) The subtraction $\chi''F_{q_\parallel=0} - \chi''F_{q_\parallel=0.64}\chi''F$ at $T = 30$ K. The line is the result of fitting to a power law $\sim\frac{1}{\omega^2}$. All data were collected at $2\theta = 150°$.

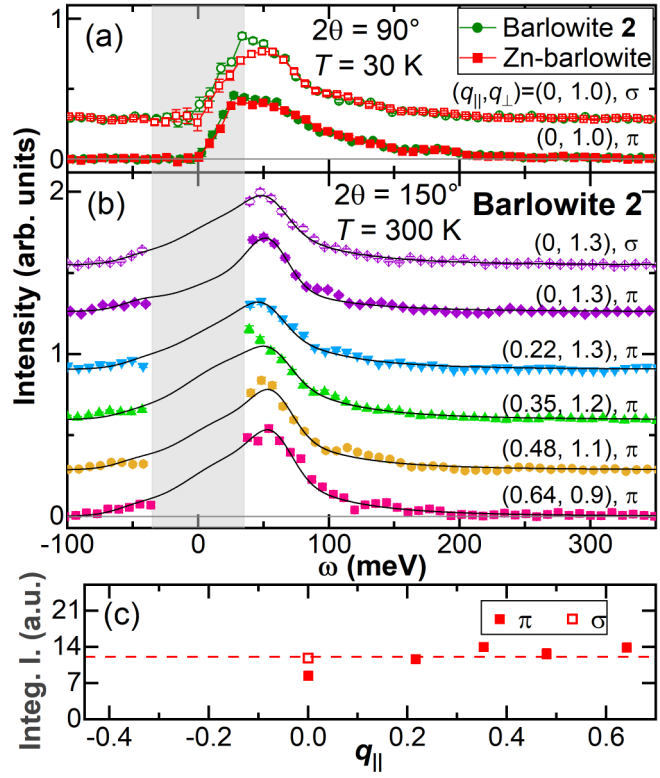

FIG. 4. (a) Comparing the inelastic scattering of Zn-barlowite $Zn_{0.56}$ and barlowite 2 collected at $q_\parallel = 0$, $T = 30$ K, and $2\theta = 90°$. The shading denotes a region of high uncertainty due to the elastic subtraction. (b) The q dependence of the inelastic scattering of barlowite 2 collected at $T = 300$ K and $2\theta = 150°$. The data were fit with the "DHO+phonon" model (SM Sec. VI); the best fits are shown as black lines. The shaded region was masked during fitting; full $T = 300$ K data are in Fig. S17. Vertical offsets were applied to separate the spectra. (c) Fitted integrated intensity as a function of $q_\parallel$. The horizontal dashed line is the average value.

interpretation in terms of scattering from pairs of spinons or spinon-antispinon pairs [25,41]. The fact that the signal extends to a high energy of $\sim 14J$ suggests that the entirety of the scattering does not arise from a single pair of spinon excitations. The high-energy tail of the RIXS scattering can be empirically fit to a power law $1/\omega^\alpha$ with $\alpha \simeq 2$, as shown in Fig. 3(c). In the context of scattering from a single spinon pair, we fit the magnetic signal in Fig. 3(c) with the functional form $S(q, \omega) = A/\omega^{2-\eta}$ used to describe possible QSL states [42–44]. The fitted η would have to be quite small (<0.25) to describe the continuum within these scenarios.

Therefore, the high-energy RIXS scattering in Zn-barlowite $Zn_{0.56}$ likely includes significant contributions from multiple spinon pairs. Since RIXS can measure spin excitations with $\Delta S = 0$, scattering from spinon-antispinon pairs may also be present. Calculations for the Raman cross section of the Dirac spin liquid on the kagome lattice are instructive: Ko *et al.* predicted a broad spectrum of scattering extending up to ~100 meV for herbertsmithite at $q = 0$, which includes significant contributions from up to three spinon-antispinon pairs [41]. Here, to describe scattering from multiple pairs of spinons and/or antispinons, we modeled the data in Fig. 3(b) with four Lorentzian peaks representing 1-pair, 2-pair, 3-pair, and 4-pair scattering. We find that the intensity of the Lorentzians decrease as $1/\omega_0^2$, where ω_0 denotes the center of each peak. The position of the 1-pair peak occurs at ~35 meV, close to the peak position seen in magnetic Raman measurements [40,45]. Interestingly, the intensity of the 1-pair peak is roughly 70% of the total spectral weight, similar to the result for the spin-$\frac{1}{2}$ chain QSL [46,47].

The presence of scattering at $q_\parallel = 0$ further supports that the signal originates from more than one spinon pair. We calculated the static spin structure factor using density matrix renormalization group techniques [48] on the $S = \frac{1}{2}$ antiferromagnetic Heisenberg model on the kagome lattice [Figs. 1(c) and S19]. The scattering, which represents the energy-integrated $\Delta S = 1$ scattering, is very weak at $q_\parallel = 0$ as expected for antiferromagnetic correlations and is not consistent with our data. However, the signal at small $q_\parallel$ may be enhanced when considering inelastic scattering from multiple pairs of spinons. We inspected the difference of the spin structure factors $dS(\mathbf{q}, S_z) = S(\mathbf{q}, S_z) - S(\mathbf{q}, 0)$, where S_z denotes

the number of pairs of spinon-spinon excitations, and find improved consistency between $dS(\mathbf{q}, 2)$ and the RIXS results (see Fig. S19). Moreover, the signal at $q_{\parallel} = 0$ may have a substantial contribution from scattering from spinon-antispinon pairs (as discussed above regarding the Raman predictions [41]); however, the RIXS cross section for these processes has not yet been calculated.

We additionally collected RIXS data on small crystals of the magnetically ordered parent compound $Cu_4(OH)_6FBr$, barlowite 2, which does not have disorder related to cation substitution [20,21]. The parent compound has $T_N \approx 10$ K and maintains hexagonal symmetry at low temperatures [21], which is distinct from the variant that becomes orthorhombic [19–21,49–52]. Figure 4(a) shows that $Zn_{0.56}$ and barlowite 2 exhibit qualitatively similar RIXS spectra at $T = 30$ K and $2\theta = 90°$; data collected at $T = 300$ K and $2\theta = 150°$ in Fig. 4(b) likewise appear similar to Zn-barlowite, exhibiting a broad continuum.

The similarity of the inelastic spectrum in barlowite 2 and Zn-barlowite $Zn_{0.56}$ indicates that spinon-based scattering can dominate at high energies even if magnetic order occurs at low temperatures. Furthermore, this shows that the high-energy dynamics are not sensitive to interlayer disorder or interactions at much smaller energy scales, which eventually play a role in the ground state physics [21]. In other systems, RIXS measurements on a $S = \frac{1}{2}$ chain compound that orders at low temperatures revealed the presence of 4-spinon scattering [25], which was more cleanly observed at the oxygen K edge, compared to the Cu L edge. Interestingly, we find sufficient signal for the multispinon scattering at the Cu L edge in this kagome system where the orbital arrangements differ significantly from the cuprates. Even in two dimensions, the ordered $S = \frac{1}{2}$ square lattice antiferromagnet shows evidence for spinon continuum excitations at high energies probed with neutrons [53]. Future studies of Zn-barlowite and barlowite at the oxygen K edge would certainly be useful to further probe the multispinon excitations [25,54].

Our data reveal that the magnetic excitations in the QSL candidate Zn-substituted barlowite forms a broad continuum extending up to $\sim 14J$. Within a QSL picture, the results indicate scattering from multiple spinon-antispinon and/or spinon-spinon pairs—a discovery made possible by the RIXS technique. Further work on understanding the multispinon excitations for the kagome QSLs (and their competing states) and calculating the appropriate RIXS cross sections would be most illuminating.

The work at Stanford and SLAC in the Stanford Institute for Materials and Energy Sciences (SIMES) was supported by the U.S. Department of Energy (DOE), Office of Science, Basic Energy Sciences (BES), Materials Sciences and Engineering Division, under Contract No. DE-AC02-76SF00515. This research used beamline 2-ID of the National Synchrotron Light Source II, a U.S. Department of Energy (DOE) Office of Science User Facility operated for the DOE Office of Science by Brookhaven National Laboratory under Contract No. DE-SC0012704. Part of this work was supported by the Laboratory Directed Research and Development project of Brookhaven National Laboratory No. 21-037. Part of this work was performed at the Stanford Nano Shared Facilities (SNSF), supported by the National Science Foundation under Award No. ECCS-2026822. R.W.S. was supported by the Department of Defense through the NDSEG Fellowship Program and by a NSF Graduate Research Fellowship (DGE-1656518). We thank Senthil Todadri and Yao Wang for helpful discussions and A. F. LaFranchi for assistance with PYTHON.

[1] L. Balents, Spin liquids in frustrated magnets, Nature (London) **464**, 199 (2010).
[2] M. R. Norman, Herbertsmithite and the search for the quantum spin liquid, Rev. Mod. Phys. **88**, 041002 (2016).
[3] C. Broholm, R. J. Cava, S. A. Kivelson, D. G. Nocera, M. R. Norman, and T. Senthil, Quantum spin liquids, Science **367**, eaay0668 (2020).
[4] S. Sachdev, Kagomé- and triangular-lattice Heisenberg antiferromagnets: Ordering from quantum fluctuations and quantum-disordered ground states with unconfined bosonic spinons, Phys. Rev. B **45**, 12377 (1992).
[5] Y. Ran, M. Hermele, P. A. Lee, and X.-G. Wen, Projected-Wave-Function Study of the Spin-1/2 Heisenberg Model on the Kagomé Lattice, Phys. Rev. Lett. **98**, 117205 (2007).
[6] H. C. Jiang, Z. Y. Weng, and D. N. Sheng, Density Matrix Renormalization Group Numerical Study of the Kagome Antiferromagnet, Phys. Rev. Lett. **101**, 117203 (2008).
[7] S. Yan, D. A. Huse, and S. R. White, Spin-liquid ground state of the $S = \frac{1}{2}$ kagome Heisenberg antiferromagnet, Science **332**, 1173 (2011).
[8] S. Depenbrock, I. P. McCulloch, and U. Schollwöck, Nature of the Spin-Liquid Ground State of the $S = 1/2$ Heisenberg Model on the Kagome Lattice, Phys. Rev. Lett. **109**, 067201 (2012).
[9] H. C. Jiang, Z. Wang, and L. Balents, Identifying topological order by entanglement entropy, Nat. Phys. **8**, 902 (2012).
[10] Y.-C. He, M. P. Zaletel, M. Oshikawa, and F. Pollmann, Signatures of Dirac Cones in a DMRG Study of the Kagome Heisenberg Model, Phys. Rev. X **7**, 031020 (2017).
[11] J.-W. Mei, J.-Y. Chen, H. He, and X.-G. Wen, Gapped spin liquid with Z_2 topological order for the kagome Heisenberg model, Phys. Rev. B **95**, 235107 (2017).
[12] H. J. Liao, Z. Y. Xie, J. Chen, Z. Y. Liu, H. D. Xie, R. Z. Huang, B. Normand, and T. Xiang, Gapless Spin-Liquid Ground State in the $S = 1/2$ Kagome Antiferromagnet, Phys. Rev. Lett. **118**, 137202 (2017).
[13] C. Zhang and T. Li, Variational study of the ground state and spin dynamics of the spin-$\frac{1}{2}$ kagome antiferromagnetic Heisenberg model and its implication for herbertsmithite $ZnCu_3(OH)_6Cl_2$, Phys. Rev. B **102**, 195106 (2020).
[14] M. P. Shores, E. A. Nytko, B. M. Bartlett, and D. G. Nocera, A structurally perfect $S = \frac{1}{2}$ kagomé antiferromagnet, J. Am. Chem. Soc. **127**, 13462 (2005).
[15] T.-H. Han, J. S. Helton, S. Chu, D. G. Nocera, J. A. Rodriguez-Rivera, C. Broholm, and Y. S. Lee, Fractionalized excitations in the spin-liquid state of a kagome-lattice antiferromagnet, Nature (London) **492**, 406 (2012).

[16] M. Fu, T. Imai, T.-H. Han, and Y. S. Lee, Evidence for a gapped spin-liquid ground state in a kagome Heisenberg antiferromagnet, Science **350**, 655 (2015).

[17] T.-H. Han, M. R. Norman, J.-J. Wen, J. A. Rodriguez-Rivera, J. S. Helton, C. Broholm, and Y. S. Lee, Correlated impurities and intrinsic spin-liquid physics in the kagome material herbertsmithite, Phys. Rev. B **94**, 060409(R) (2016).

[18] J. Wang, W. Yuan, P. M. Singer, R. W. Smaha, W. He, J. Wen, Y. S. Lee, and T. Imai, Emergence of spin singlets with inhomogeneous gaps in the kagome lattice Heisenberg antiferromagnets Zn-barlowite and herbertsmithite, Nat. Phys. **17**, 1109 (2021).

[19] Z. Feng, Y. Wei, R. Liu, D. Yan, Y.-C. Wang, J. Luo, A. Senyshyn, C. Cruz, W. Yi, J.-W. Mei, Z. Y. Meng, Y. Shi, and S. Li, Effect of Zn doping on the antiferromagnetism in kagome $Cu_{4-x}Zn_x(OH)_6FBr$, Phys. Rev. B **98**, 155127 (2018).

[20] R. W. Smaha, W. He, J. P. Sheckelton, J. Wen, and Y. S. Lee, Synthesis-dependent properties of barlowite and Zn-substituted barlowite, J. Solid State Chem. **268**, 123 (2018).

[21] R. W. Smaha, W. He, J. M. Jiang, J. Wen, Y. F. Jiang, J. P. Sheckelton, C. J. Titus, S. G. Wang, Y. S. Chen, S. J. Teat, A. A. Aczel, Y. Zhao, G. Xu, J. W. Lynn, H. C. Jiang, and Y. S. Lee, Materializing rival ground states in the barlowite family of kagome magnets: Quantum spin liquid, spin ordered, and valence bond crystal states, npj Quantum Mater. **5**, 23 (2020).

[22] R. W. Smaha, I. Boukahil, C. J. Titus, J. M. Jiang, J. P. Sheckelton, W. He, J. Wen, J. Vinson, S. G. Wang, Y.-S. Chen, S. J. Teat, T. P. Devereaux, C. D. Pemmaraju, and Y. S. Lee, Site-specific structure at multiple length scales in kagome quantum spin liquid candidates, Phys. Rev. Mater. **4**, 124406 (2020).

[23] See Supplemental Material at http://link.aps.org/supplemental/10.1103/PhysRevB.107.L060402 for further information about data collection and analysis; a comparison with calculated phonons; additional data for Zn-barlowite showing temperature dependence, specular subtractions, and the conversion to $\chi''F$; additional data on barlowite; a comparison of Zn-barlowite and barlowite; and additional DMRG calculations, which also includes Refs. [55–57].

[24] L. J. P. Ament, M. van Veenendaal, T. P. Devereaux, J. P. Hill, and J. van den Brink, Resonant inelastic x-ray scattering studies of elementary excitations, Rev. Mod. Phys. **83**, 705 (2011).

[25] J. Schlappa, U. Kumar, K. J. Zhou, S. Singh, M. Mourigal, L. Patthey, H. M. Rønnow, S. Johnston, and T. Schmitt, Probing multi-spinon excitations outside of the two-spinon continuum in the antiferromagnetic spin chain cuprate Sr_2CuO_3, Nat. Commun. **9**, 5394 (2018).

[26] J. Pelliciari, S. Lee, K. Gilmore, J. Li, Y. Gu, A. Barbour, I. Jarrige, C. H. Ahn, F. J. Walker, and V. Bisogni, Tuning spin excitations in magnetic films by confinement, Nat. Mater. **20**, 188 (2021).

[27] J. Pelliciari, S. Karakuzu, Q. Song, R. Arpaia, A. Nag, M. Rossi, J. Li, T. Yu, X. Chen, R. Peng, M. García-Fernández, A. C. Walters, Q. Wang, J. Zhao, G. Ghiringhelli, D. Feng, T. A. Maier, K.-J. Zhou, S. Johnston, and R. Comin, Evolution of spin excitations from bulk to monolayer FeSe, Nat. Commun. **12**, 3122 (2021).

[28] A. Nag, H. C. Robarts, F. Wenzel, J. Li, H. Elnaggar, R. P. Wang, A. C. Walters, M. García-Fernández, F. M. F. de Groot, M. W. Haverkort, and K. J. Zhou, Many-Body Physics of Single and Double Spin-Flip Excitations in NiO, Phys. Rev. Lett. **124**, 067202 (2020).

[29] L. J. P. Ament, G. Ghiringhelli, M. M. Sala, L. Braicovich, and J. van den Brink, Theoretical Demonstration of How the Dispersion of Magnetic Excitations in Cuprate Compounds can be Determined using Resonant Inelastic X-Ray Scattering, Phys. Rev. Lett. **103**, 117003 (2009).

[30] L. Braicovich, M. Moretti Sala, L. J. P. Ament, V. Bisogni, M. Minola, G. Balestrino, D. Di Castro, G. M. De Luca, M. Salluzzo, G. Ghiringhelli, and J. van den Brink, Momentum and polarization dependence of single-magnon spectral weight for Cu L_3-edge resonant inelastic x-ray scattering from layered cuprates, Phys. Rev. B **81**, 174533 (2010).

[31] M. W. Haverkort, Theory of Resonant Inelastic X-Ray Scattering by Collective Magnetic Excitations, Phys. Rev. Lett. **105**, 167404 (2010).

[32] Y. Y. Peng, E. W. Huang, R. Fumagalli, M. Minola, Y. Wang, X. Sun, Y. Ding, K. Kummer, X. J. Zhou, N. B. Brookes, B. Moritz, L. Braicovich, T. P. Devereaux, and G. Ghiringhelli, Dispersion, damping, and intensity of spin excitations in the monolayer $(Bi, Pb)_2(Sr, La)_2CuO_{6+\delta}$ cuprate superconductor family, Phys. Rev. B **98**, 144507 (2018).

[33] S. H. Chun, J.-W. Kim, J. Kim, H. Zheng, C. C. Stoumpos, C. D. Malliakas, J. F. Mitchell, K. Mehlawat, Y. Singh, Y. Choi, T. Gog, A. Al-Zein, M. Moretti Sala, M. Krisch, J. Chaloupka, G. Jackeli, G. Khaliullin, and B. J. Kim, Direct evidence for dominant bond-directional interactions in a honeycomb lattice iridate Na_2IrO_3, Nat. Phys. **11**, 462 (2015).

[34] J. Kim, J. Chaloupka, Y. Singh, J. W. Kim, B. J. Kim, D. Casa, A. Said, X. Huang, and T. Gog, Dynamic Spin Correlations in the Honeycomb Lattice Na_2IrO_3 Measured by Resonant Inelastic X-Ray Scattering, Phys. Rev. X **10**, 021034 (2020).

[35] B. W. Lebert, S. Kim, V. Bisogni, I. Jarrige, A. M. Barbour, and Y. J. Kim, Resonant inelastic x-ray scattering study of α-$RuCl_3$: A progress report, J. Phys.: Condens. Matter **32**, 144001 (2020).

[36] H. Suzuki, H. Liu, J. Bertinshaw, K. Ueda, H. Kim, S. Laha, D. Weber, Z. Yang, L. Wang, H. Takahashi, K. Fürsich, M. Minola, B. V. Lotsch, B. J. Kim, H. Yavaş, M. Daghofer, J. Chaloupka, G. Khaliullin, H. Gretarsson, and B. Keimer, Proximate ferromagnetic state in the Kitaev model material α-$RuCl_3$, Nat. Commun. **12**, 4512 (2021).

[37] J. Dvorak, I. Jarrige, V. Bisogni, S. Coburn, and W. Leonhardt, Towards 10 meV resolution: The design of an ultrahigh resolution soft x-ray RIXS spectrometer, Rev. Sci. Instrum. **87**, 115109 (2016).

[38] M. W. Haverkort, N. Hollmann, I. P. Krug, and A. Tanaka, Symmetry analysis of magneto-optical effects: The case of x-ray diffraction and x-ray absorption at the transition metal $L_{2,3}$ edge, Phys. Rev. B **82**, 094403 (2010).

[39] J. Wang, W. Yuan, P. M. Singer, R. W. Smaha, W. He, J. Wen, Y. S. Lee, and T. Imai, Freezing of the Lattice in the Kagome Lattice Heisenberg Antiferromagnet Zn-Barlowite $ZnCu_3(OD)_6FBr$, Phys. Rev. Lett. **128**, 157202 (2022).

[40] Y. Fu, M.-L. Lin, L. Wang, Q. Liu, L. Huang, W. Jiang, Z. Hao, C. Liu, H. Zhang, X. Shi, J. Zhang, J. Dai, D. Yu, F. Ye, P. A. Lee, P.-H. Tan, and J.-W. Mei, Dynamic fingerprint of fractionalized excitations in single-crystalline $Cu_3Zn(OH)_6FBr$, Nat. Commun. **12**, 3048 (2021).

[41] W.-H. Ko, Z.-X. Liu, T.-K. Ng, and P. A. Lee, Raman signature of the U(1) Dirac spin-liquid state in the spin-$\frac{1}{2}$ kagome system, Phys. Rev. B **81**, 024414 (2010).

[42] M. Hermele, Y. Ran, P. A. Lee, and X.-G. Wen, Properties of an algebraic spin liquid on the kagome lattice, Phys. Rev. B **77**, 224413 (2008).

[43] A. V. Chubukov, T. Senthil, and S. Sachdev, Universal Magnetic Properties of Frustrated Quantum Antiferromagnets in Two Dimensions, Phys. Rev. Lett. **72**, 2089 (1994).

[44] R. Coldea, D. A. Tennant, and Z. Tylczynski, Extended scattering continua characteristic of spin fractionalization in the two-dimensional frustrated quantum magnet Cu_2CuCl_4 observed by neutron scattering, Phys. Rev. B **68**, 134424 (2003).

[45] D. Wulferding, P. Lemmens, P. Scheib, J. Röder, P. Mendels, S. Chu, T. Han, and Y. S. Lee, Interplay of thermal and quantum spin fluctuations in the kagome lattice compound herbertsmithite, Phys. Rev. B **82**, 144412 (2010).

[46] M. Karbach, G. Müller, A. H. Bougourzi, A. Fledderjohann, and K.-H. Mütter, Two-spinon dynamic structure factor of the one-dimensional $s = \frac{1}{2}$ Heisenberg antiferromagnet, Phys. Rev. B **55**, 12510 (1997).

[47] M. Mourigal, M. Enderle, A. Klöpperpieper, J.-S. Caux, A. Stunault, and H. M. Rønnow, Fractional spinon excitations in the quantum Heisenberg antiferromagnetic chain, Nat. Phys. **9**, 435 (2013).

[48] S. R. White, Density Matrix Formulation for Quantum Renormalization Groups, Phys. Rev. Lett. **69**, 2863 (1992).

[49] T.-H. Han, J. Singleton, and J. A. Schlueter, Barlowite: A Spin-1/2 Antiferromagnet with a Geometrically Perfect Kagome Motif, Phys. Rev. Lett. **113**, 227203 (2014).

[50] H. O. Jeschke, F. Salvat-Pujol, E. Gati, N. H. Hoang, B. Wolf, M. Lang, J. A. Schlueter, and R. Valentí, Barlowite as a canted antiferromagnet: Theory and experiment, Phys. Rev. B **92**, 094417 (2015).

[51] C. M. Pasco, B. A. Trump, T. T. Tran, Z. A. Kelly, C. Hoffmann, I. Heinmaa, R. Stern, and T. M. McQueen, Single-crystal growth of $Cu_4(OH)_6BrF$ and universal behavior in quantum spin liquid candidates synthetic barlowite and herbertsmithite, Phys. Rev. Mater. **2**, 044406 (2018).

[52] A. Henderson, L. Dong, S. Biswas, H. I. Revell, Y. Xin, R. Valenti, A. Schlueter, and T. Siegrist, Order–disorder transition in the $S = \frac{1}{2}$ kagome antiferromagnets claringbullite and barlowite, Chem. Commun. **55**, 11587 (2019).

[53] B. Dalla Piazza, M. Mourigal, N. B. Christensen, G. J. Nilsen, P. Tregenna-Piggott, T. G. Perring, M. Enderle, D. F. McMorrow, D. A. Ivanov, and H. M. Rønnow, Fractional excitations in the square-lattice quantum antiferromagnet, Nat. Phys. **11**, 62 (2015).

[54] Z. Xiong, T. Datta, and D.-X. Yao, Resonant inelastic x-ray scattering study of vector chiral ordered kagome antiferromagnet, npj Quantum Mater. **5**, 78 (2020).

[55] I. Jarrige, V. Bisogni, Y. Zhu, W. Leonhardt, and J. Dvorak, Paving the way to ultra-high-resolution resonant inelastic x-ray scattering with the SIX Beamline at NSLS-II, Synchrotron Radiat. News **31**, 7 (2018).

[56] M. Newville, R. Otten, A. Nelson, A. Ingargiola, T. Stensitzki, D. Allan, A. Fox, F. Carter, Michał, D. Pustakhod, lneuhaus, S. Weigand, R. Osborn, Glenn, C. Deil, Mark, A. L. R. Hansen, G. Pasquevich, L. Foks, N. Zobrist *et al.*, lmfit/lmfit-py 1.0.2 (2020).

[57] E. T. Abel, K. Matan, F. C. Chou, E. D. Isaacs, D. E. Moncton, H. Sinn, A. Alatas, and Y. S. Lee, X-ray scattering study of the spin-Peierls transition and soft phonon behavior in TiOCl, Phys. Rev. B **76**, 214304 (2007).